Valley filter and valley valve based on WSe_2 double-barrier junctions modulated by polarized light

Danna Liu,[1] Boyao Liu,[1] Ruiyang Yuan,[2,*] Jun Zheng,[3] and Yong Guo[1,†]

[1]*Department of Physics and State Key Laboratory of Low-Dimensional Quantum Physics, Tsinghua University, Beijing 100084, People's Republic of China*

[2]*Center for Theoretical Physics, Department of Physics, Capital Normal University, Beijing 100048, People's Republic of China*

[3]*School of Mathematics and Physics, Bohai University, Jinzhou 121013, People's Republic of China*

(Received 18 November 2020; revised 14 May 2021; accepted 7 June 2021; published 24 June 2021)

We demonstrate that an off-resonant circularly polarized light-modulated double-barrier monolayer WSe_2 junction can operate as a valley filter and a valley valve simultaneously. Spin-, valley-, and energy-dependent line-type resonant peaks appear in the transmission spectrum, and the splitting of the valley degree of freedom due to the coupling between the light-induced gap and the valley index is also present. By fixing the light on the first barrier, the valley switch can be controlled efficiently by the optical field on the second one. Furthermore, the gate voltage can adjust not only the conductance but also the operation window of the valley filter. The proposed junction provides insight into the manipulation of valley degree of freedom based on WSe_2 and other transition metal dichalcogenides.

DOI: 10.1103/PhysRevB.103.245432

I. INTRODUCTION

The emergence of high-quality monolayer WSe_2 [1] with an enormous direct band gap in the visible range [2] and strong spin-orbit coupling (SOC) [3] superior to graphene [4–8] and silicene [9,10] has triggered broad research about its application in spintronics and valleytronics [11–15]. The inequivalent K valley and K' valley located at the edges of the conductance and valence bands in the first Brillouin zone are connected by the time reversal symmetry and can be broken by helicity of light [16]. The chiral electronic states are also predicted to possess valley-contrasting orbital magnetic moments coupling valley pseudospin to magnetic fields, which opens up the possibility of magnetic control over the valley degree of freedom [17–24]. On the other hand, the strong SOC can be used to achieve spin manipulation when bulk or thin WSe_2 is exfoliated into a monolayer [25]. There are several corresponding works both in theory and experiment [26–28] on manipulating spin and valley. Such examples include the peculiar magnetic field [29], which causes Zeeman splitting into the boundary states of different valleys; the magnetic insulator deposited on WSe_2 using the proximity effect to induce magnetism [30]; and the pseudomagnetic field originating from the circularly polarized light (CPL) by utilizing the optical Stark effect [31–36] to select one of the two inequivalent valleys. Recently, Li *et al.* found that fully valley- and spin-polarized conductance can be achieved in a ferromagnetic MoS_2 junction [13]. In off-resonant CPL-modulated two-dimensional (2D) systems, Zhai and Jin found that the topological phase transition between the band insulator and Floquet topological insulator can be induced in epitaxial graphene [37]. In addition, the spin-valley current can be controlled in a double ferromagnetic barrier silicene junction under the application of CPL [38]. However, what we should emphasize is that the K' valley cannot be completely filtered in such a structure, and the range of the light frequency window to realize the valley valve is very narrow. Tahir *et al.* studied the CPL's impact on the valley-dependent transport in monolayer MoS_2 and showed that CPL could lead to perfect valley polarization by tuning the band gap [39]. Hajati *et al.* proposed a ferromagnetic MoS_2 junction with CPL on the FM region. They found that the valley- and spin-polarized currents can be simultaneously attained due to the decrease of the degeneracies [40]. Although some of the properties of the 2D materials subjected to CPL have been well studied, the attention given to the tunneling properties and the optically controlled valley switch in double-barrier transition metal dichalcogenides (TMDs) is extremely limited.

This work demonstrates a CPL-modulated double-barrier junction based on monolayer WSe_2 which can simultaneously serve as a valley filter and valley valve. We find that line-type resonant peaks and the splitting of the valley degree of freedom are present in the transmission spectrum. We show that when the CPL is tuned in such a way that the wave vectors along the x axis in the two barrier regions are both real, the device can operate as a valley filter; however, if one of the two wave vectors is complex, the device can operate as a perfect valley valve. We further show that the gate voltage can adjust the conductance and valley filter's operation window. Our research may provide some new ideas for the practical application of TMD-based optoelectronic devices.

II. MODEL AND METHODS

We propose a CPL-modulated valley filter and valley valve device based on a monolayer WSe_2 double-barrier structure.

*yuanry@cnu.edu.cn
†guoy66@mail.tsinghua.edu.cn

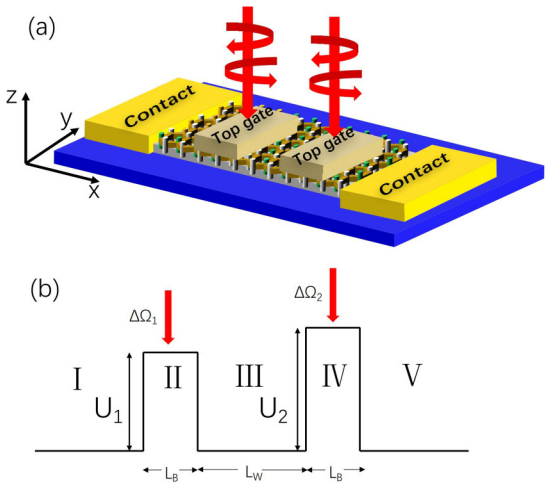

FIG. 1. (a) Schematic diagram of the valley filter and valley valve device with CPL applied to the two barrier regions. The CPL in region II produces the valley-polarized particles due to the coupling between the valley index and the light-induced gap of CPL, while the CPL in region IV acts as a switch to control the passage of the valley-polarized particles. The gate voltage can be used to adjust the operation window of the valley switch and the conductance. (b) The schematic potential of the model. $U_{1(2)}$ are the heights of barriers; L_B and L_W are the barrier thickness and well width, respectively.

As shown in Fig. 1, the monolayer WSe_2 strip mechanically exfoliated from bulk WSe_2 is placed on the Si/SiO_2 substrate [41] in the x-y plane, and the device is in contact with the Ti/Au electrode to transfer the carrier between the electrode and WSe_2. The potential barriers of height U_1 and U_2 are separated by a well with width L_W, and such local barriers can be implemented by electric fields perpendicular to the WSe_2 plane. The adjustment of the optical field to the valley filter can be achieved by applying the CPL vertically on the two barrier regions. The nontransparent sheets are introduced to the normal regions to ensure that the light field can be applied independently to the barrier. A similar approach was proposed by Borghardt *et al.* [42]. What must be mentioned is that the carrier diffusion length measured in monolayer WSe_2 is 380 nm [43], so we limit the junction length to less than 380 nm in the following calculation to make the transport ballistic, so that only elastic scattering occurs. Although the size of the device used in our calculation is very small, our results are still applicable to large size structures within the ballistic transport range.

The low-energy 2D Dirac-like Hamiltonian of monolayer WSe_2 in our proposed structure describing the massive fermions with strong SOC is [44]

$$H_{\eta,s_z} = \hbar\upsilon_f(\eta\sigma_x p_x + \sigma_y p_y) + (\Delta \pm \eta\Delta\Omega)\sigma_z + \eta s_z(\lambda_c\sigma_+ + \lambda_v\sigma_-) + U, \quad (1)$$

where $\upsilon_f = 5\times10^5$ m/s is the Fermi velocity. σ_i $(i = x, y, z)$ is the Pauli matrix, with $\sigma_\pm = \sigma_0 \pm \sigma_z$ (σ_0 is the unity matrix). $\lambda_v = 112.5$ meV is the SOC for the valence band, and $\lambda_c = 7.5$ meV for the conduction band. $p_i (i = x, y)$ is the momentum operator, $\Delta = 850$ meV is the band gap. $\eta = 1$ (-1) denotes the K (K') valley, and $s_z = 1$ (-1) corresponds to spin up (down). U is the electric potential induced by the gate voltage.

The circularly polarized light can be represented by the magnetic vector potential: $A(t) = (\pm A\sin\Omega t, A\cos\Omega t)$, where A and Ω correspond to the amplitude of the potential and the frequency of light, respectively. The effect of off-resonant circularly polarized light on the systems can be reduced to the static effective Hamiltonian by Floquet theory when $\hbar\Omega \gg t$ ($t = 1.19$ eV is the hopping parameter between the two nearest neighbors) is satisfied [3]; only optical fields in the high-frequency region meet this condition. There is no optical absorption, and the light does not directly excite the electrons and instead effectively modifies the electron band structure through a virtual photon absorption/emission process. Additionally, in the limit of $eA\upsilon_f/\hbar\Omega \ll 1$, the static effective Hamiltonian around the Dirac point has the form of $\pm\eta\Delta\Omega\sigma_z$, where $\Delta\Omega = (eA\upsilon_f)^2/\hbar\Omega$ is the light-induced gap of the CPL and $+$ and $-$ correspond to the right-handed and left-handed polarization, respectively. The lowest light frequency that satisfies this condition is 10^{15} Hz, determined by the bandwidth ($2\Delta = 1.7$ eV $= \hbar\Omega$). For $\Omega = 1.4\times10^{15}$ Hz and $\Delta\Omega = 100$ meV, the real laser intensity $I \approx 10^{15}$ W m^{-2} [45].

The wave equation in each region can be expressed in the following form:

$$\begin{aligned}
\Psi_I &= \begin{pmatrix} 1 \\ \frac{\hbar\upsilon_f(-\eta k_x - ik_y)}{\delta} \end{pmatrix} e^{ik_x x} + r\begin{pmatrix} 1 \\ \frac{\hbar\upsilon_f(\eta k_x - ik_y)}{\delta} \end{pmatrix} e^{-ik_x x}, \\
\Psi_{II} &= a_2\begin{pmatrix} 1 \\ \frac{\hbar\upsilon_f(-\eta k_x' - ik_y)}{\delta_1} \end{pmatrix} e^{ik_x' x} + b_2\begin{pmatrix} 1 \\ \frac{\hbar\upsilon_f(\eta k_x' - ik_y)}{\delta_1} \end{pmatrix} e^{-ik_x' x}, \\
\Psi_{III} &= a_3\begin{pmatrix} 1 \\ \frac{\hbar\upsilon_f(-\eta k_x - ik_y)}{\delta} \end{pmatrix} e^{ik_x x} + b_3\begin{pmatrix} 1 \\ \frac{\hbar\upsilon_f(\eta k_x - ik_y)}{\delta} \end{pmatrix} e^{-ik_x x}, \quad (2) \\
\Psi_{IV} &= a_4\begin{pmatrix} 1 \\ \frac{\hbar\upsilon_f(-\eta k_x'' - ik_y)}{\delta_2} \end{pmatrix} e^{ik_x'' x} + b_4\begin{pmatrix} 1 \\ \frac{\hbar\upsilon_f(\eta k_x'' - ik_y)}{\delta_2} \end{pmatrix} e^{-ik_x'' x}, \\
\Psi_V &= t_{\eta s_z}\begin{pmatrix} 1 \\ \frac{\hbar\upsilon_f(-\eta k_x - ik_y)}{\delta} \end{pmatrix} e^{ik_x x},
\end{aligned}$$

where we set $\delta_{1(2)} = -\Delta - \eta\Delta\Omega_{1(2)} + 2\eta s_z\lambda_v + U_{1(2)} - E$, $\delta = -\Delta + 2\eta s_z\lambda_v - E$. r, a_i, and b_i $(i = 2, 3, 4)$ are the scattering coefficients. The parallel and perpendicular wave vectors in each region are

$$\begin{aligned}
k_y &= \frac{\sqrt{(\eta s_z\lambda_+ - E)^2 - (\Delta + \eta s_z\lambda_-)^2}}{\hbar\upsilon_f}\sin\theta, \\
k_x^2 &= \frac{(\eta s_z\lambda_+ - E)^2 - (\Delta + \eta s_z\lambda_-)^2}{(\hbar\upsilon_f)^2} - k_y^2, \\
k_x'^2 &= \frac{(\eta s_z\lambda_+ + U_1 - E)^2 - (\Delta + \eta\Delta\Omega_1 + \eta s_z\lambda_-)^2}{(\hbar\upsilon_f)^2} - k_y^2, \\
k_x''^2 &= \frac{(\eta s_z\lambda_+ + U_2 - E)^2 - (\Delta + \eta\Delta\Omega_2 + \eta s_z\lambda_-)^2}{(\hbar\upsilon_f)^2} - k_y^2.
\end{aligned} \quad (3)$$

The energy dispersion relation in the modulated regions is

$$E_\pm = \pm\sqrt{(\Delta + \eta\Delta\Omega + \eta s_z\lambda_-)^2 + \hbar^2\upsilon_f^2 k^2} + \eta s_z\lambda_+ + U, \quad (4)$$

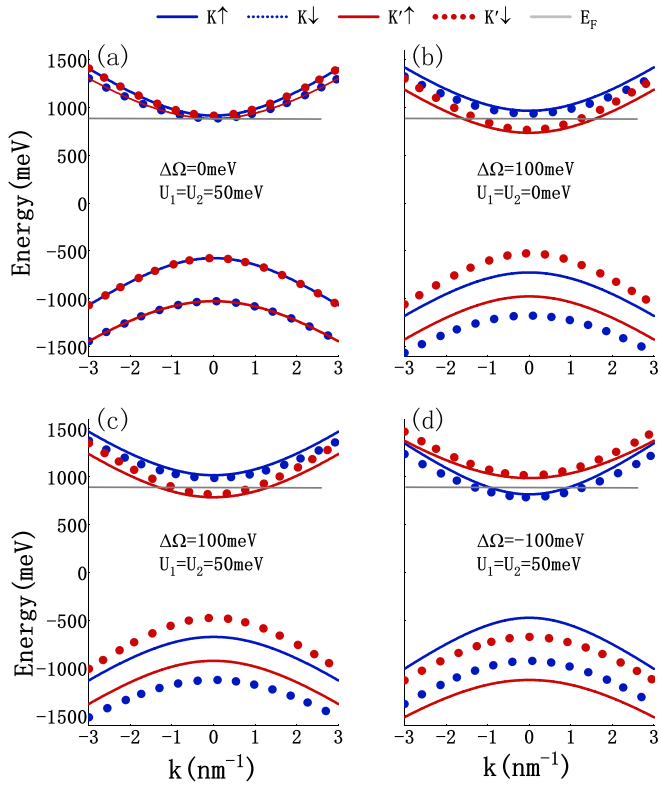

FIG. 2. Band structures in the barrier region. The gray line represents the Fermi energy level; here we set the Fermi energy level as $E_F = 900$ meV, and the other parameters are labeled.

where $\lambda_\pm = \lambda_c \pm \lambda_v$ and k is the wave vector. In the normal regions, the eigenvalue can be expressed by setting $U = 0$ meV and $\Delta\Omega = 0$ meV in Eq. (4).

Using the continuity condition of the wave function at the interfaces of regions I–V [see Fig. 1(b)], the spin- and valley-dependent coefficients $t_{\eta s_z}$ can be obtained with

$$\begin{aligned}\Psi_I(x=0) &= \Psi_{II}(x=0),\\ \Psi_{II}(x=L_B) &= \Psi_{III}(x=L_B),\\ \Psi_{III}(x=L_B+L_W) &= \Psi_{IV}(x=L_B+L_W),\\ \Psi_{IV}(x=2L_B+L_W) &= \Psi_V(x=2L_B+L_W).\end{aligned} \tag{5}$$

The spin- and valley-dependent transmission probability can be calculated through the transfer-matrix method: $T_{\eta s_z} = |t_{\eta s_z}|^2$. The conductance at zero temperature is given by the Landauer-Büttiker formula [46]:

$$G_{\eta s_z} = G_0 \int T_{\eta s_z} \cos\theta d\theta, \tag{6}$$

where θ denotes the incident angle and $G_0 = 2e^2/h$ is the quantum conductance. The valley-resolved conductance is $G_{K(K')} = (G_{K(K')\uparrow} + G_{K(K')\downarrow})/2$. The total conductance is $G_t = G_K + G_{K'}$, and the corresponding valley polarization is defined as $P_V = (G_K - G_{K'})/G_t$.

III. RESULTS AND DISCUSSION

In Fig. 2, we depict the influence of the CPL and gate voltage on the band structure of the barrier region. It is seen that the CPL lifts both the spin and valley degeneracy. The right CPL enhances the band gap of the K valley but reduces that of the K' valley [see Figs. 2(a) and 2(c)]. The situation is just the opposite for the left CPL [see Fig. 2(d)]. The mechanism of the valley filter/valve requires different gaps in the two valleys and a Fermi level that cuts the bands of one valley but not the other. Furthermore, the gate voltage can change the position of the entire band structure relative to the Fermi level without changing the band gap; that is, the band structures shift up as a whole when U increases from 0 to 50 meV [see Figs. 2(b) and 2(c)].

In Fig. 3, we theoretically analyze the influence of some parameters, including the strength of the optical field, the number of barriers, the barrier height, and the barrier width, on the transport properties from the perspective of transmission. The decrease of valley degeneracy due to the coupling between the light-induced gap of the right CPL and the valley index can be seen clearly in Figs. 3(a) and 3(b), in which the transmission of K valley electrons is greatly suppressed, while that of the K' valley electrons is enhanced. In addition, there is a striking difference in tunneling transmission between the single barrier and the double barrier. The transmission spectra of the double-barrier structure show several ideal line-type resonant peaks with unity value in the low-energy region under the modulation of the optical field [see Fig. 3(d)]. The reason is the transmission coefficient is related to the propagation modes in both the barrier and the well region, in which the nonresonant region stems from the evanescent modes in the barrier region, while the line-type peaks come from the quasibound state in the well. In contrast, the line-type resonant peaks are completely absent in the single-barrier structure, which makes the double barrier superior to the single barrier in some functions.

To understand the influence of the barrier height on the transport properties, we proceed to focus on the difference in transmission spectra at various gate voltages. By increasing the barrier height from 0 to 50 meV, the transmission spectra show distinct resonant suppression [see Figs. 3(f) and 3(h)], which results in broader nonresonant regions and more ideal line-type resonant peaks. However, we find that the barrier width does not change the transmission behavior significantly [see Figs. 3(d) and 3(f)].

To illustrate how the particles are controlled by the parameters more intuitively, we show the valley-resolved conductance under various parameters, which are labeled in Fig. 4. The above results for the enhancement (suppression) of the right CPL on the K' (K) valley particles are clearly reflected in the valley-resolved conductance. It is observed that the K-valley-resolved conductance drops dramatically to zero in a wide Fermi energy region, while the K'-valley-resolved conductance is greatly enhanced to its maximum under the modulation of the right CPL. Our calculation also shows that the gate voltage has a significant effect on the oscillation behavior. That is, with the increase of the gate voltage, the transmission spectra as a whole exhibit remarkable resonant suppression behavior [see Figs. 4(b) and 4(e)]. Unlike the CPL that is coupled with the valley index, the gate voltage has the same effect on all the degrees of freedom, so the gate voltage just regulates the position of the entire band structure relative to the Fermi level. Furthermore, changing

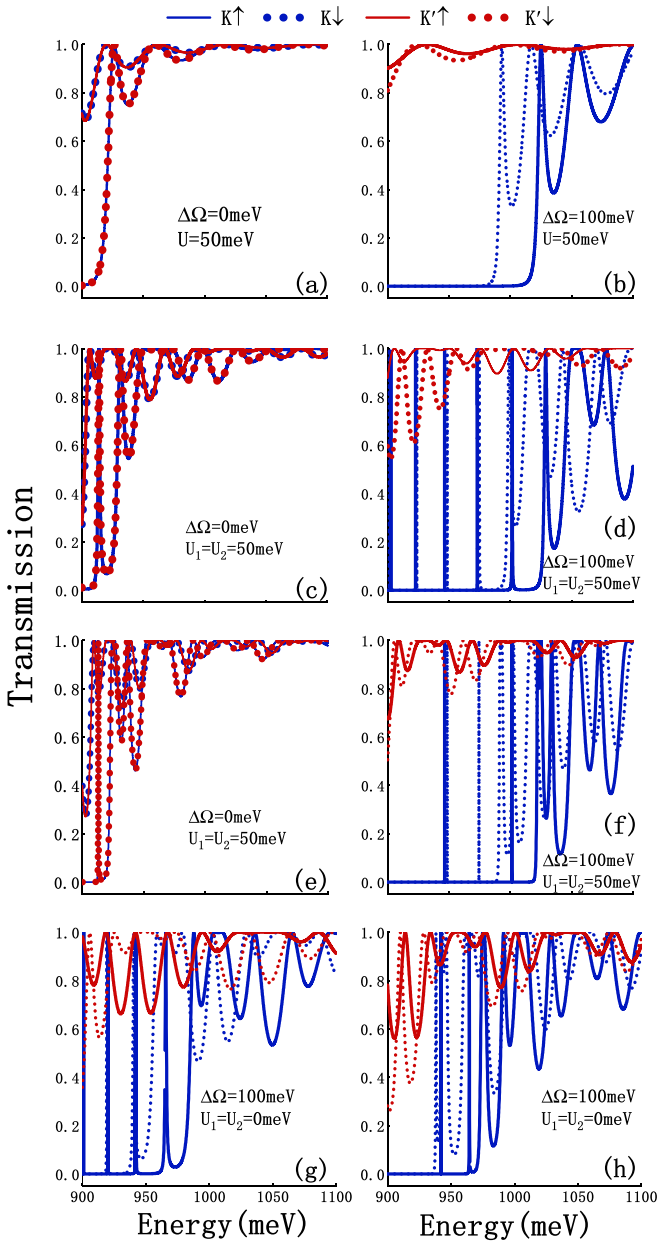

FIG. 3. The transmission as a function of the incident energy when $\theta = 0$. (a) and (b) Single-barrier structure and (c)–(h) double-barrier structure. L_B and L_W indicate the widths of the barrier and the well, respectively. (a) and (b) $L_B = 7.8$ nm, (c), (d), and (g) $L_B = 3.9$ nm, $L_W = 15.6$ nm, (e), (f) and (h) $L_B = 7.8$ nm, $L_W = 15.6$ nm. The other parameters are labeled. K (K') ↑ and K (K') ↓ represent the K (K') valley electrons with spin up and spin down, respectively.

the barrier width has little effect on the transmission of the system [see Figs. 4(b) and 4(d)]. The control of gate voltage is also necessary for valleytronics applications. Figure 5 shows the impact of gate voltage on both the total conductance and the valley-resolved conductance at several light-induced gaps of the CPL when $E_F = 900$ meV [Figs. 5(a)–5(c)] and $E_F = 1100$ meV [Figs. 5(d)–5(f)]. As can be seen in Fig. 5(a), when $E_F = 900$ meV, the total conductance increases first and then declines with U, and the tuning point is at $U = \Delta\Omega$. To explain this phenomenon, we calculate the valley conductance as

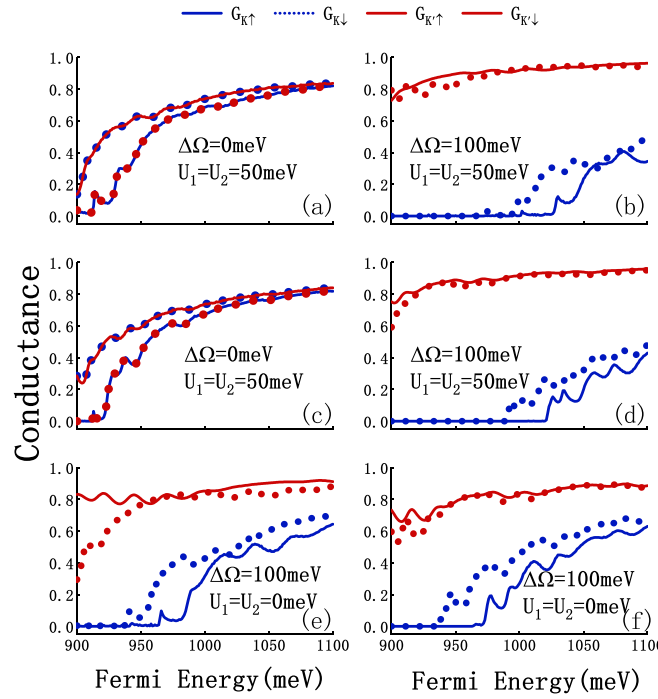

FIG. 4. Valley-resolved conductance as a function of the Fermi energy. (a), (b), and (e) $L_B = 3.9$ nm, $L_W = 15.6$ nm; (c), (d), and (f) $L_B = 7.8$ nm, $L_W = 15.6$ nm. The other parameters are labeled.

a function of gate voltage [see Figs. 5(b) and 5(c)]. Due to the suppressed effect of CPL with right-handed polarization on K-valley-dependent electrons, the K'-valley-dependent conductance makes a major contribution to the total conductance. The reason why the tuning point is limited to $U = \Delta\Omega$ is

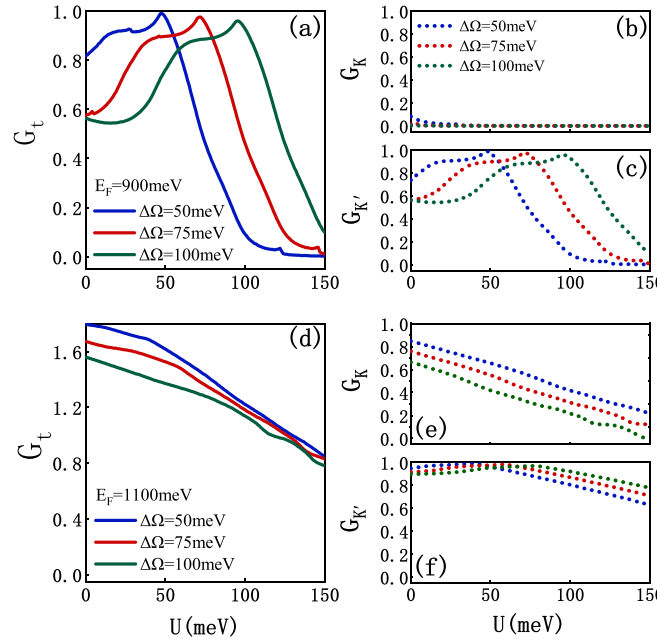

FIG. 5. Total conductance and valley-resolved conductance as a function of the gate voltage at several light-induced gaps of the CPL. (a)–(c) $E_F = 900$ meV and (d)–(f) $E_F = 1100$ meV. $L_B = 3.9$ nm, and $L_W = 15.6$ nm.

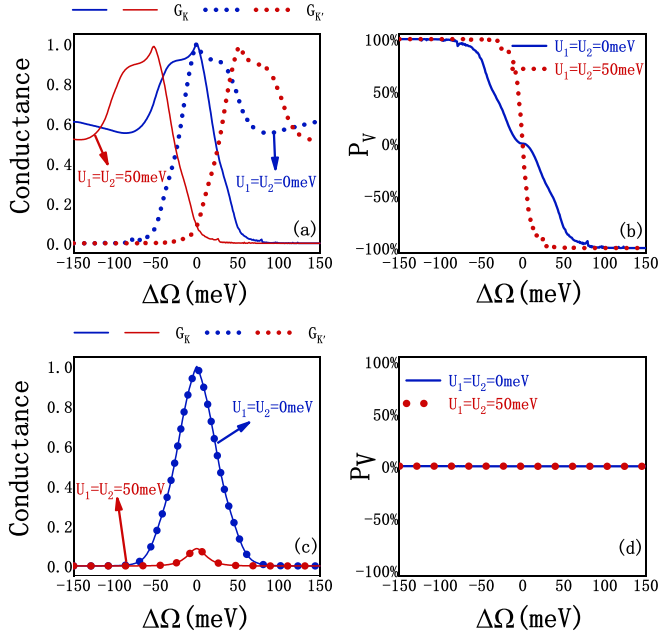

FIG. 6. The valley filter and valley valve effects of the symmetric structure. Valley-resolved conductance and valley polarization are displayed as a function of the light-induced gap of the CPL at various values of the height of barrier. (a) and (b) $\Delta\Omega_1 = \Delta\Omega_2$ and (c) and (d) $\Delta\Omega_1 = -\Delta\Omega_2$. The incident energy is 900 meV.

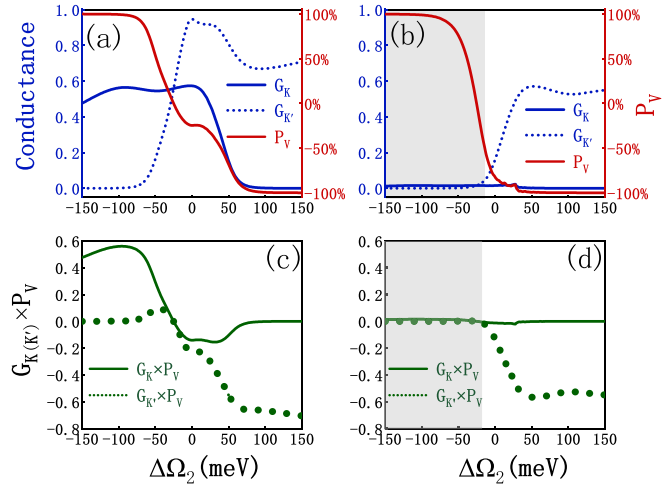

FIG. 7. The valley filter and the valley valve effects of the asymmetric structure. (a) and (b) Valley-resolved conductance and valley polarization and (c) and (d) the product of valley-resolved conductance and valley polarization as a function of the light-induced gap of the CPL on the second barrier when $\Delta\Omega_1 = 25$ meV. The shaded area in (b) and (d) represent the area where the value of the vertical coordinates approaches zero. The parameters are $U_1 = U_2 = 0$ meV for the left panels and $U_1 = U_2 = 50$ meV for the right panels. The incident energy is 900 meV.

due to the best matching of the K'-valley-dependent band structures between the modulated and normal regions in this case. For the case of $E_F = 1100$ meV as shown in Fig. 5(d), however, the total conductance decreases with the gate voltage, and the increase of the light-induced gap of the CPL has a pronounced suppression effect on the total conductance. For $E_F = 1100$ meV, the total conductance is larger than that when $E_F = 900$ meV. The higher conductance at large Fermi energies is due to the higher transmission at high energies.

Next, we discuss the valley filter and valley valve effects of the symmetrically modulated structure, which means that the intensities of the CPL on the two barriers are the same. In Fig. 6, we present the valley-resolved conductance and valley polarization as a function of the light-induced gap of the CPL for different values of the gate voltage when $\Delta\Omega_1 = \Delta\Omega_2$ for Figs. 6(a) and 6(b) and $\Delta\Omega_1 = -\Delta\Omega_2$ for Figs. 6(c) and 6(d), and the incident energy is 900 meV. By adjusting the intensity of the optical field on the two barriers, the function of a valley filter can be realized [see Figs. 6(a) and 6(b)]. Moreover, it is worth mentioning that compared with $U_1 = U_2 = 0$ meV, the operation window of the valley filter when $U_1 = U_2 = 50$ meV becomes wider; the reason is that the increase of gate voltage leads to the movement of K-resolved conductance towards the low-energy region, while the K'-resolved conductance moves towards the high-energy region.

We now consider the valley valve effects of the device. In Figs. 6(c) and 6(d), we show the valley-resolved conductance and valley polarization as a function of the light-induced gap of the CPL when the polarizations of the CPL on the two barriers are opposite. A significant change is clearly seen; that is, there is no decrease of valley degeneracy. Thus, one can achieve the valley valve effect. Furthermore, when U increases from 0 to 50 meV, the total conductance drops significantly, even approaching zero in the vast range of the optical intensity. Therefore, if $U_1 = U_2 = 50$ meV is selected, we can directly judge that the corresponding device can be used to realize the valley valve function from the sharp decrease of conductance when adjusting the light-induced gap of the CPL from $\Delta\Omega_1 = \Delta\Omega_2$ to $\Delta\Omega_1 = -\Delta\Omega_2$.

The valley filter and valley valve effects of the asymmetric structure are shown in Fig. 7. Here the asymmetrically modulated structure means that the CPLs on the two barriers are different in strength. We calculate the valley-resolved conductance, the valley polarization, and the product of valley-resolved conductance and valley polarization versus $\Delta\Omega_2$ (while fixing $\Delta\Omega_1 = 25$ meV) for $U_1 = U_2 = 0$ meV (left panels) and $U_1 = U_2 = 50$ meV (right panels); the incident energy is 900 meV. As can be seen from the valley polarization diagram [see Fig. 7(a)], the asymmetrical structure can also be used to realize the function of the valley switch.

Figures 7(c) and 7(d) show the product of valley-resolved conductance and valley polarization. There are three cases where the product of valley conductance and valley polarization tends to zero: valley-resolved conductance is very small, valley polarization is very imperfect, or both are very low. From the perspective of the experimental value, these three cases have no experimental significance, so they can be regarded as the operating window of valley valves. When $U_1 = U_2 = 0$ meV [see Fig. 7(c)], one of the two valley-resolved conductances has a distinct value at a particular optical frequency, so the actual operation window of the valley switch is consistent with the calculated result. When $U_1 = U_2 = 50$ meV [see Fig. 7(d)], the shaded region indicates

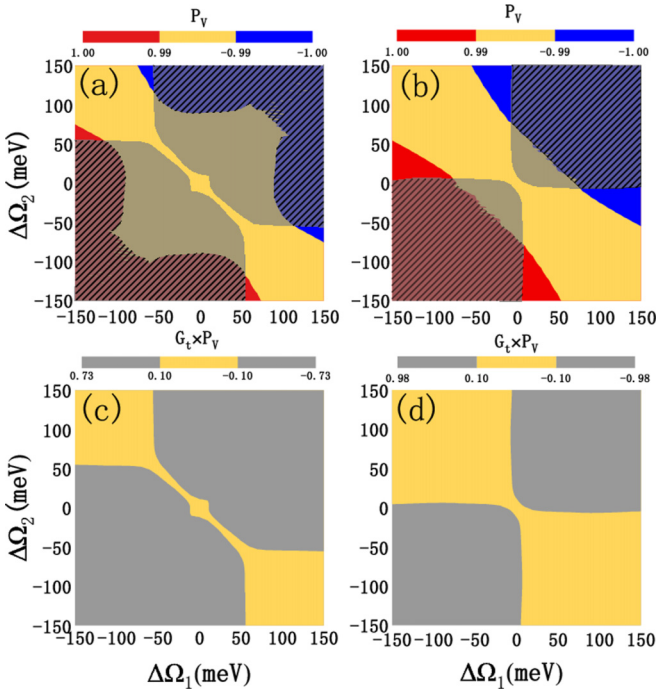

FIG. 8. (a) and (b) Valley polarization and (c) and (d) the product of total conductance and valley polarization as a function of the light-induced gap of the CPL on the two barrier regions. The parameters are $U_1 = U_2 = 0$ meV for the left panels and $U_1 = U_2 = 50$ meV for the right panels. The incident energy is 900 meV.

that the product of valley-resolved conductance and valley polarization is very low, so this region is actually the region for realizing the valley valve.

The influences of gate voltage and the strength and polarization of light on the valley switch function can be intuitively seen from Fig. 8. The red and blue parts in Figs. 8(a) and 8(b) represent the operation window with perfect valley polarization, and the gray shaded parts in Figs. 8(c) and 8(d) represent the product of total conductance and valley polarization not close to zero. The oblique part obtained after the coincidence of the two is the valley filter window with experimental significance. The principle of the valley switch can be explained in terms of wave vectors along the x axis. Assuming that k_x' or k_x'' [see Eq. (3)] in the modulated region is real, the wave in the barrier region is oscillating, and the coupling of the oscillating waves between the two barrier regions results in extremely high transmission. On the other hand, if k_x' or k_x'' is imaginary, the evanescent wave in the modulated region suppresses the transport. When the gate voltage and the CPL are tuned such that the waves of the K (K') valley particles are simultaneously oscillating, the junction will filter out the K (K') valley.

IV. CONCLUSIONS

In summary, we proposed an off-resonant circularly polarized light-modulated and gate voltage-modulated monolayer WSe_2 double barrier to function as a valley filter and valley valve device. It was found that not only the spin-, valley-, and energy-dependent line-type resonant peaks but also the splitting of the valley degree of freedom is present in the transmission spectrum. We pointed out that the valley switch can be controlled efficiently by the CPL applied to the double barriers, and we attribute such remarkable results to the coupling of the waves along the x axis in the two barrier regions. Specifically, the gate voltage can adjust the conductance and the operation window of the valley filter. Our findings may be useful for the practical application of photoelectric devices based on transition metal dichalcogenides.

The data supporting the findings of this study are available from the corresponding author upon request.

ACKNOWLEDGMENTS

This work was supported by the National Nature Science Foundation of China (Grants No. 12071209 and No. 11804236) and the General Program of Science and Technology Development Project of the Beijing Municipal Education Commission of China under Grant No. KM201810028005.

[1] A. M. Jones, H. Y. Yu, J. S. Ross, P. Klement, N. J. Ghimire, J. Q. Yan, D. G. Mandrus, W. Yao, and X. D. Xu, Nat. Phys. **10**, 130 (2014).
[2] W. T. Hsu, L. S. Lu, D. Wang, J. K. Huang, M. Y. Li, T. R. Chang, Y. C. Chou, Z. Y. Juang, H. T. Jeng, L. J. Li, and W. H. Chang, Nat. Commun. **8**, 929 (2017).
[3] D. Xiao, G. B. Liu, W. X. Feng, X. D. Xu, and W. Yao, Phys. Rev. Lett. **108**, 196802 (2012).
[4] J. C. Boettger and S. B. Trickey, Phys. Rev. B **75**, 121402(R) (2007).
[5] A. H. Castro Neto, F. Guinea, N. M. R. Peres, K. S. Novoselov, and A. K. Geim, Rev. Mod. Phys. **81**, 109 (2009).
[6] M. I. Katsnelson, K. S. Novoselov, and A. K. Geim, Nat. Phys. **2**, 620 (2006).
[7] D. W. Zhai and N. Sandler, Phys. Rev. B **98**, 165437 (2018).
[8] T. Stegmann and N. Szpak, 2D Mater. **6**, 015024 (2018).
[9] N. D. Drummond, V. Zólyomi, and V. I. Fal'ko, Phys. Rev. B **85**, 075423 (2012).
[10] Z. P. Niu and S. H. Dong, Europhys. Lett. **111**, 37007 (2015).
[11] A. Pulkin and O. V. Yazyev, Phys. Rev. B **93**, 041419(R) (2016).
[12] Y. C. Cheng, Q. Y. Zhang, and U. Schwingenschlögl, Phys. Rev. B **89**, 155429 (2014).
[13] H. Li, J. M. Shao, D. X. Yao, and G. W. Yang, ACS Appl. Mater. Interfaces **6**, 1759 (2014).
[14] P. M. Krstajić, P. Vasilopoulos, and M. Tahir, Phys. E (Amsterdam, Neth.) **75**, 317 (2016).
[15] R. Y. Yuan, Q. J. Yang, and Y. Guo, J. Phys.: Condens. Matter **30**, 355301 (2018).
[16] A. M. Jones, H. Y. Yu, N. J. Ghimire, S. F. Wu, G. Aivazian, J. S. Ross, B. Zhao, J. Q. Yan, D. G. Mandrus, D. Xiao, W. Yao, and X. D. Xu, Nat. Nanotechnol. **8**, 634 (2013).
[17] W. Yao, D. Xiao, and Q. Niu, Phys. Rev. B **77**, 235406 (2008).
[18] D. Xiao, W. Yao, and Q. Niu, Phys. Rev. Lett. **99**, 236809 (2007).
[19] A. Kormányos, V. Zólyomi, N. D. Drummond, and G. Burkard, Phys. Rev. X **4**, 011034 (2014).

[20] X. Li, F. Zhang, and Q. Niu, Phys. Rev. Lett. **110**, 066803 (2013).
[21] R. L. Chu, X. Li, S. F. Wu, Q. Niu, W. Yao, X. D. Xu, and C. W. Zhang, Phys. Rev. B **90**, 045427 (2014).
[22] H. Rostami, A. G. Moghaddam, and R. Asgari, Phys. Rev. B **88**, 085440 (2013).
[23] Y. H. Ho, Y. H. Wang, and H. Y. Chen, Phys. Rev. B **89**, 155316 (2014).
[24] T. Y. Cai, S. A. Yang, X. Li, F. Zhang, J. R. Shi, W. Yao, and Q. Niu, Phys. Rev. B **88**, 115140 (2013).
[25] Z. Y. Zhu, Y. C. Cheng, and U. Schwingenschlögl, Phys. Rev. B **84**, 153402 (2011).
[26] A. Srivastava, M. Sidler, A. V. Allain, D. S. Lembke, A. Kis, and A. Imamoğlu, Nat. Phys. **11**, 141 (2015).
[27] H. T. Yuan, X. Q. Wang, B. Lian, H. J. Zhang, X. F. Fang, B. Shen, G. Xu, Y. Xu, S. C. Zhang, H. Y. Hwang, and Y. Cui, Nat. Nanotechnol. **9**, 851 (2014).
[28] Q. J. Yang, R. Y. Yuan, and Y. Guo, J. Phys. D **52**, 335301 (2019).
[29] D. MacNeill, C. Heikes, K. F. Mak, Z. Anderson, A. Kormányos, V. Zólyomi, J. Park, and D. C. Ralph, Phys. Rev. Lett. **114**, 037401 (2015).
[30] C. Zhao, T. Norden, P. Y. Zhang, P. Q. Zhao, Y. C. Cheng, F. Sun, J. P. Parry, P. Taheri, J. Q. Wang, and Y. Yang, Nat. Nanotechnol. **12**, 757 (2017).
[31] T. Cao, G. Wang, W. P. Han, H. Q. Ye, C. R. Zhu, J. R. Shi, Q. Niu, P. H. Tan, E. G. Wang, B. L. Liu, and J. Feng, Nat. Commun. **3**, 887 (2012).
[32] K. F. Mak, K. L. He, J. Shan, and T. F. Heinz, Nat. Nanotechnol. **7**, 494 (2012).
[33] H. L. Zeng, J. F. Dai, W. Yao, D. Xiao, and X. D. Cui, Nat. Nanotechnol. **7**, 490 (2012).
[34] F. H. Qi, J. Cao, and G. J. Jin, Phys. Rev. B **98**, 045422 (2018).
[35] H. Bao, W. H. Liao, X. C. Zhang, H. Yang, X. X. Yang, and H. P. Zhao, J. Appl. Phys. **121**, 205106 (2017).
[36] X. J. Qiu, Z. Z. Cao, J. M. Lei, J. Shen, and C. C. Qin, Superlattices Microstruct. **109**, 735 (2017).
[37] X. C. Zhai and G. J. Jin, Phys. Rev. B **89**, 235416 (2014).
[38] P. Chantngarm, K. Yamada, and B. Soodchomshom, J. Magn. Magn. Mater. **429**, 16 (2017).
[39] M. Tahir, A. Manchon, and U. Schwingenschlögl, Phys. Rev. B **90**, 125438 (2014).
[40] Y. Hajati, Z. Amini, and M. Sabaeian, J. Magn. Magn. Mater. **503**, 166580 (2020).
[41] M. Koperski, K. Nogajewski, A. Arora, V. Cherkez, P. Mallet, J. Y. Veuillen, J. Marcus, P. Kossacki, and M. Potemski, Nat. Nanotechnol. **10**, 503 (2015).
[42] S. Borghardt, J. Sonntag, J. S. Tu, T. Taniguchi, K. Watanabe, B. Beschoten, C. Stampfer, and B. E. Kardynal, Opt. Mater. Express **10**, 1273 (2020).
[43] Q. N. Cui, F. Ceballos, N. Kumar, and H. Zhao, ACS Nano **8**, 2970 (2014).
[44] M. Tahir, Phys. E (Amsterdam, Neth.) **97**, 184 (2018).
[45] J. Atteia, J. H. Bardarson, and J. Cayssol, Phys. Rev. B **96**, 245404 (2017).
[46] M. Büttiker, Phys. Rev. Lett. **57**, 1761 (1986).